PTEP

Prog. Theor. Exp. Phys. **2015**, 00000 (22 pages)
DOI: 10.1093/ptep/0000000000

arXiv:1606.00362v1 [astro-ph.HE] 1 Jun 2016

Gravitational wave quasinormal mode from Population III massive black hole binaries in various models of population synthesis

Tomoya Kinugawa[1], Hiroyuki Nakano[2] and Takashi Nakamura[2]

[1]*Institute for Cosmic Ray Research, The University of Tokyo, Chiba 277-8582, Japan*
[2]*Department of Physics, Kyoto University, Kyoto 606-8502, Japan*

Focusing on the remnant black holes after merging binary black holes, we show that ringdown gravitational waves of Population III binary black holes mergers can be detected with the rate of $5.9-500$ events yr^{-1} (SFR$_{\rm p}$/($10^{-2.5}$ $M_\odot$ yr^{-1} Mpc^{-3})) $\cdot$ ([f$_{\rm b}$/(1 + f$_{\rm b}$)]/0.33) for various parameters and functions. This rate is estimated for the events with SNR$>$ 8 for the second generation gravitational wave detectors such as KAGRA. Here, SFR$_{\rm p}$ and f$_{\rm b}$ are the peak value of the Population III star formation rate and the fraction of binaries, respectively. When we consider only the events with SNR$>$ 35, the event rate becomes $0.046-4.21$ events yr^{-1} (SFR$_{\rm p}$/($10^{-2.5}$ $M_\odot$ yr^{-1} Mpc^{-3})) $\cdot$ ([f$_{\rm b}$/(1 + f$_{\rm b}$)]/0.33). This suggest that for remnant black hole's spin $q_f > 0.95$ we have the event rate with SNR$>$ 35 less than 0.037 events yr^{-1} (SFR$_{\rm p}$/($10^{-2.5}$ $M_\odot$ yr^{-1} Mpc^{-3})) $\cdot$ ([f$_{\rm b}$/(1 + f$_{\rm b}$)]/0.33), while it is $3-30$ events yr^{-1} (SFR$_{\rm p}$/($10^{-2.5}$ $M_\odot$ yr^{-1} Mpc^{-3})) $\cdot$ ([f$_{\rm b}$/(1 + f$_{\rm b}$)]/0.33) for the third generation detectors such as Einstein Telescope. If we detect many Population III binary black holes merger, it may be possible to constrain the Population III binary evolution paths not only by the mass distribution but also by the spin distribution.

Subject Index E31, E02, E01, E38

1. Introduction

The final part of gravitational waves (GWs) from merging binary black holes (BBHs) is called the ringdown phase. When the remnant compact object is a black hole (BH), this phase is described by quasinormal modes (QNMs) of the BH (see. e.g., Ref. [1]). In general, the BH is expected as the Kerr spacetime [2],

$$\begin{aligned} ds^2 &= -\left(1-\frac{2Mr}{\Sigma}\right)dt^2 - \frac{4Mar\sin^2\theta}{\Sigma}dtd\phi + \frac{\Sigma}{\Delta}dr^2 \\ &\quad +\Sigma d\theta^2 + \left(r^2+a^2+\frac{2Ma^2r}{\Sigma}\sin^2\theta\right)\sin^2\theta d\phi^2\,, \end{aligned} \tag{1}$$

where $\Delta = r^2 - 2Mr + a^2$ and $\Sigma = r^2 + a^2\cos^2\theta$. with mass M and spin a. The detection of QNM GWs is not only to give a precise estimation of the BH's mass and spin, but also to test Einstein's general relativity (see an extensive review [3]).

In our previous paper [4], using the recent population synthesis results of Population III (Pop III) massive BBHs [5, 6], we discussed the event rate of the QNM GWs by the second generation gravitational wave detectors such as Advanced LIGO (aLIGO) [7], Advanced Virgo (AdV) [8], and KAGRA [9, 10]. Since there are various parameters and functions

© The Author(s) 2012. Published by Oxford University Press on behalf of the Physical Society of Japan.
This is an Open Access article distributed under the terms of the Creative Commons Attribution License (http://creativecommons.org/licenses/by-nc/3.0), which permits unrestricted use, distribution, and reproduction in any medium, provided the original work is properly cited.

in the population synthesis calculation, we extensively examine BBH binary formations in this paper. Then, we calculate the remnant BH's mass M_f and the non-dimensional spin $q_f = a_f/M_f$ via fitting formulas [11], and the event rate for each model.

This paper is organized as follows. In Sec. 2, we summarize our Pop III binary population synthesis calculation, and prepare 10 models. In Sec. 3, we show the mass ratio distributions of BBH remnants for each model. The dependences on initial distribution functions, binary parameters etc. are discussed there. In Sec. 4, we obtain the spin distributions of BBH remnants for various parameters. Using the results presented in the above sections, we calculate the mass and spin distributions of the remnant BHs after merger in Sec. 5, and show the event rates of QNMs for each mode in KAGRA. Final section 6 is devoted to discussions.

2. Population III binary population synthesis calculation

To estimate the detection rate of GWs from Pop III BBH mergers, it is necessary to know how many Pop III binaries become BBHs which merge within the Hubble time. Here, we use the binary population synthesis method which is the Monte Carlo simulation of binary evolutions. The Pop III binary population synthesis code [4–6] has been upgraded from the binary population synthesis code [12, 13] for Pop III binaries. In this paper, we calculate the same models as Ref. [6] using the same methods as Ref. [6] in order to obtain the mass ratio distribution and the spin distribution. In this section, we review the calculation method and models. Note that in this paper, we do not consider the kick models and the worst model discussed in Ref. [6] for simplicity, because in these models, BBHs have misaligned spins and the final spins after merger are too complex.

First, we need to give initial conditions when a binary is born. The initial conditions such as primary mass M_1, mass ratio M_2/M_1 where M_2 is the secondary mass, separation a and orbital eccentricity e are decided by Monte Carlo method with initial distribution functions such as the initial mass function (IMF), the initial mass ratio function (IMRF), the initial separation function (ISF), and the initial eccentricity function (IEF). For example, in our standard model, we use the flat IMF, the flat IMRF, the logflat ISF and the IEF with a function of $\propto e$. There is no observation of Pop III binary because they born at the early universe. Thus, we do not know the initial distribution functions of Pop III binaries from the observation. For the IMF, however, the recent simulations [14, 15] may suggest the flat IMF. Therefore, we adapt the flat IMF. For the other initial distribution functions, we adapt those of Pop I case where Pop I star is solar like star. The set of the above initial distribution functions is called as our standard model in this paper.

Second, we calculate the evolution of each star, and if the star satisfies a condition of binary interactions, we evaluate the effects of binary interactions and change M_1, M_2, a and e. As the binary interactions, we treat the Roche lobe overflow (RLOF), the common envelope (CE) phase, the tidal effect, the supernova effect, and the gravitational radiation. The RLOF is the stable mass transfer, while the unstable mass transfer becomes the CE phase when the donor star is a giant. Here, we need some parameters for the calculation of the RLOF and the CE phase.

In the case of the RLOF, we use the lose fraction β of transfered stellar matter defined as

$$\dot{M}_2 = -(1-\beta)\dot{M}_1 \,. \tag{2}$$

where $\dot{M}_2$ is the mass accretion rate of a receiver star, $\dot{M}_1$ is the mass loss rate of a donor star. In our standard model, β is determined by the Hurley's function [12] which has been discussed for the Pop I case. When the receiver star is in the main sequence phase or in the He-burning phase, we assume that the accretion rate is described by

$$\dot{M}_2 = -\min\left(10\frac{\tau_{\dot{M}}}{\tau_{\rm KH,2}}, 1\right)\dot{M}_1\,, \tag{3}$$

where $\tau_{\dot{M}}$ is the accretion time scale defined by

$$\tau_{\dot{M}} \equiv \frac{M_2}{\dot{M}_1}\,, \tag{4}$$

and the Kelvin-Helmholtz timescale $\tau_{\rm KH,2}$ is defined by

$$\tau_{\rm KH,2} = \frac{GM_2(M_2 - M_{\rm c,2})}{L_2 R_2}\,. \tag{5}$$

Here, M_2, $M_{\rm c,2}$, L_2 and R_2 are the mass, the core mass, the luminosity and the radius of the receiver star, respectively. When the receiver star is in the He-shell burning phase, we assume that the receiver star can get all transfered matter from the donor star, i.e.,

$$\dot{M}_2 = -\dot{M}_1\,. \tag{6}$$

Although we use the β function defined by Hurley et al. [12] in our standard model, we also treat the accretion rate of the receiver star described by the constant β parameter. This is because the accretion rate of the receiver star which is not a compact object, is not understood well. Furthermore, in our previous study [6], we have shown that the Hurley fitting formula is consistent with $\beta = 0$ in the Pop III binary case. Thus, we also discuss the cases of $\beta = 0.5$ and $\beta = 1$. It is noted that the stability of the mass transfer changes if the mass transfer is nonconservative ($\beta > 0$). We use the criterion given in Ref. [16] as

$$\begin{aligned}\zeta_{\rm L} &= \frac{d\log R_{\rm L,1}}{d\log M_1} \\ &= \left[\left(0.33 + 0.13\frac{M_1}{M_2}\right)\left(1 + \frac{M_1}{M_2} - \beta\frac{M_1}{M_2}\right) + (1-\beta)\left(\left(\frac{M_1}{M_2}\right)^2 - 1\right)\right. \\ &\quad \left. - \beta\frac{M_1}{M_2}\right] \Big/ \left(1 + \frac{M_1}{M_2}\right)\,,\end{aligned} \tag{7}$$

where M_1 and $R_{\rm L,1}$ are the mass and the Roche lobe radius of the donor star. If $\zeta_{\rm ad} = d\log R_{\rm ad,1}/d\log M_1 < \zeta_{\rm L}$ where $R_{\rm ad,1}$ is the radius of the donor star, in the hydrostatic equilibrium of the donor star, the binary starts a dynamically unstable mass transfer such as the CE phase. When the receiver star is a compact object such as a neutron star and a BH, we always use $\beta = 0$ and the upper limit of the accretion rate is limited by the Eddington accretion rate defined by

$$\begin{aligned}\dot{M}_{\rm Edd} &= \frac{4\pi c R_2}{\kappa_{\rm T}} \\ &= 2.08\times10^{-3}\,(1+X)^{-1}\left(\frac{R_2}{R_\odot}\right)\ M_\odot\ {\rm yr}^{-1}\,,\end{aligned} \tag{8}$$

where $\kappa_{\rm T} = 0.2\,(1+X)$ cm^2 g^{-1} is the Thomson scattering opacity and $X(=0.76)$ is the H-mass fraction for Pop III stars.

Table 1: The model parameters in this paper. Each column represents the model name, the initial mass function (IMF), the initial eccentricity function (IEF), the common envelope (CE) parameter $\alpha\lambda$, and the lose fraction β of transfer of stellar matter at the Roche lobe overflow (RLOF) in each model.

Model	IMF	IEF	$\alpha\lambda$	β
our standard	flat	e	1	function
IMF: logflat	M^{-1}	e	1	function
IMF: Salpeter	Salpeter	e	1	function
IEF: const.	flat	const.	1	function
IEF: $e^{-0.5}$	flat	$e^{-0.5}$	1	function
$\alpha\lambda = 0.01$	flat	e	0.01	function
$\alpha\lambda = 0.1$	flat	e	0.1	function
$\alpha\lambda = 10$	flat	e	10	function
$\beta = 0.5$	flat	e	1	0.5
$\beta = 1$	flat	e	1	1

At the CE phase, the companion star plunges into the envelope of the donor star and spiral in. The orbital separation after the CE phase $a_{\rm f}$ is calculated by the energy formalism [17] which is described by

$$\alpha\left(\frac{GM_{\rm c,1}M_2}{2a_{\rm f}} - \frac{GM_1M_2}{2a_{\rm i}}\right) = \frac{GM_1M_{\rm env,1}}{\lambda R_1}\,, \tag{9}$$

where $a_{\rm i}$, α and λ are the orbital separation before the CE phase, the efficiency and the binding energy parameter, respectively. In our standard model, we adopt $\alpha\lambda = 1$. We also calculate the $\alpha\lambda = 0.01$, 0.1 and 10 cases in this paper.

Finally, if a binary becomes a BBH, we calculate the merger time which is calculated from gravitational radiation reaction, and check whether the BBH can merge within the Hubble time or not. We repeat these calculations and take the statistics of BBH mergers.

To study the dependence of Pop III BBHs properties on initial distribution functions and binary parameters, we calculate 10 models with the Pop III binary population synthesis method [5, 6] in this paper. Table 1 shows that initial distribution functions and the binary parameters of each model. The columns show the model name, the IMF, the IEF, the CE parameter $\alpha\lambda$, and the lose fraction β of transfered stellar matter at the RLOF in each model.

3. The mass ratio distributions of binary black hole remnants

Figures 1–5 show the initial mass ratio distributions and the mass ratio distributions of merging BBHs. The RLOF tends to make binaries to be equal mass. Thus, the BBHs mass ratio distributions depend on how many binaries evolve via the RLOF. The Pop III stars with mass $< 50\ M_\odot$ evolve as a blue giant. Thus, in the case of the IMF that light stars are majority, the binaries tend to evolve only via the RLOF, not via the CE phase. Therefore, the steeper IMFs tend to derive many equal mass BBHs. In this calculation, since we adopt the minimum mass ratio as $10M_\odot/M_1$, the initial mass ratio distribution of models with the IMF that light stars are majority, is upward to $M_2/M_1 = 1$ ab initio (see Figs. 1 and 2).

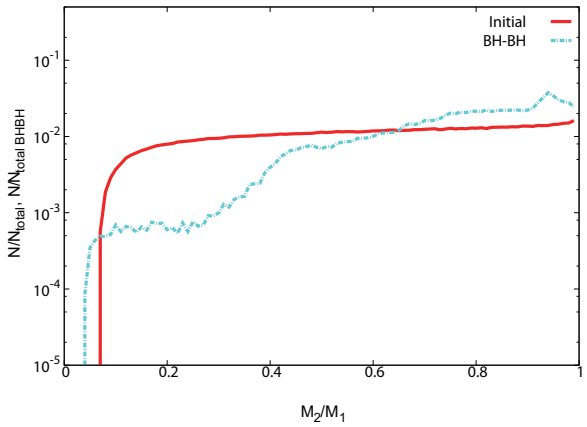

Fig. 1: The distribution of mass ratio $M_2/M_1 \leq 1$ for our standard model. The distributions of the initial mass ratio and the one when the binaries become BBHs which merge within the Hubble time, are shown as red and light blue lines, respectively. The initial mass ratio distribution is normalized by the total binary number $N_{\rm total} = 10^6$, while the one when the binaries become merging BBHs is normalized by the total merging binary number $N_{\rm total\,BHBH} = 128897$.

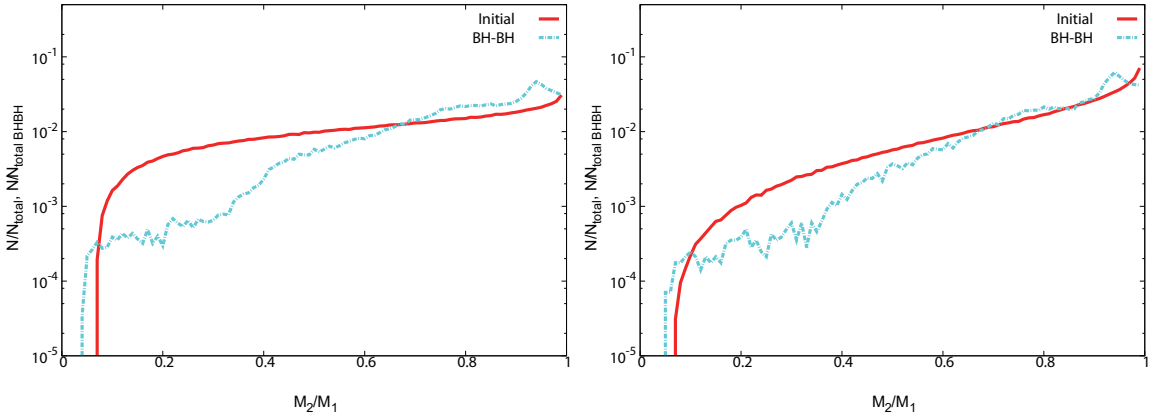

Fig. 2: The distributions of mass ratio $M_2/M_1 \leq 1$ for IMF: logflat model (left) and IMF: Salpeter model (right). The figures are same as Figure 1 but for IMF: logflat model and IMF: Salpeter model.

On the other hand, if we change the IEF, the mass ratio distribution does not change much. Thus, the dependence of IEF is not so large (see Figs. 1 and 3).

As for the CE parameter dependence (see Figs. 1 and 4), small mass ratio binaries in the model of $\alpha\lambda = 0.001$ are much fewer than those in the other models. In the $\alpha\lambda = 0.001$ model, all the binaries which evolve via the CE phase, merge during the CE phase due to too small $\alpha\lambda$. Thus, the merging BBHs in this model evolve only via the RLOF, and become equal mass by the RLOF. There is not large change between the models with the CE parameters $\alpha\lambda = 0.1$ and 10.

As for the mass loss fraction β (see Figs. 1 and 5), when β becomes large, there are three effects. First, binaries tend not to become a CE phase. Second, the mass accretion by a

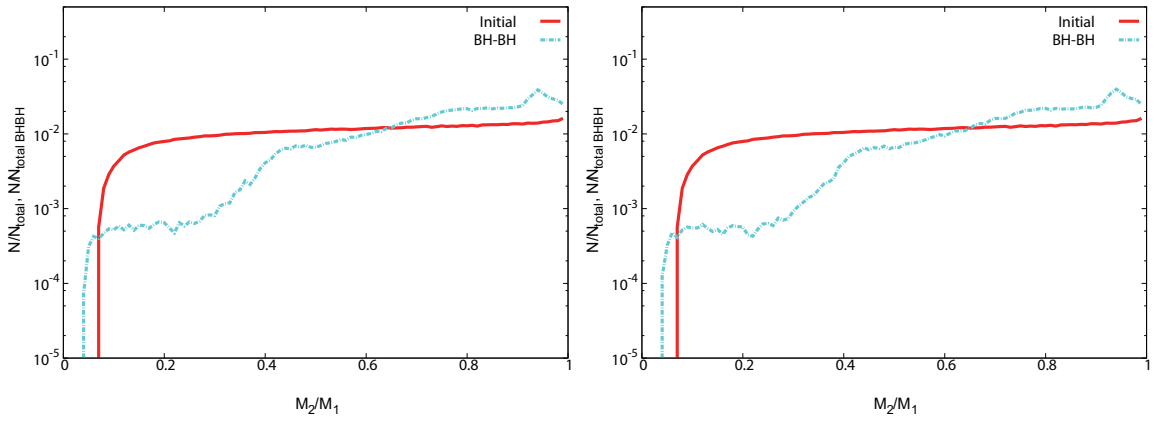

Fig. 3: The distributions of mass ratio $M_2/M_1 \leq 1$ for IEF: e = const. model (left) and IEF: $e^{-0.5}$ model (right). The figures are same as Figure 1 but for IEF: e = const. model and IEF: $e^{-0.5}$ model.

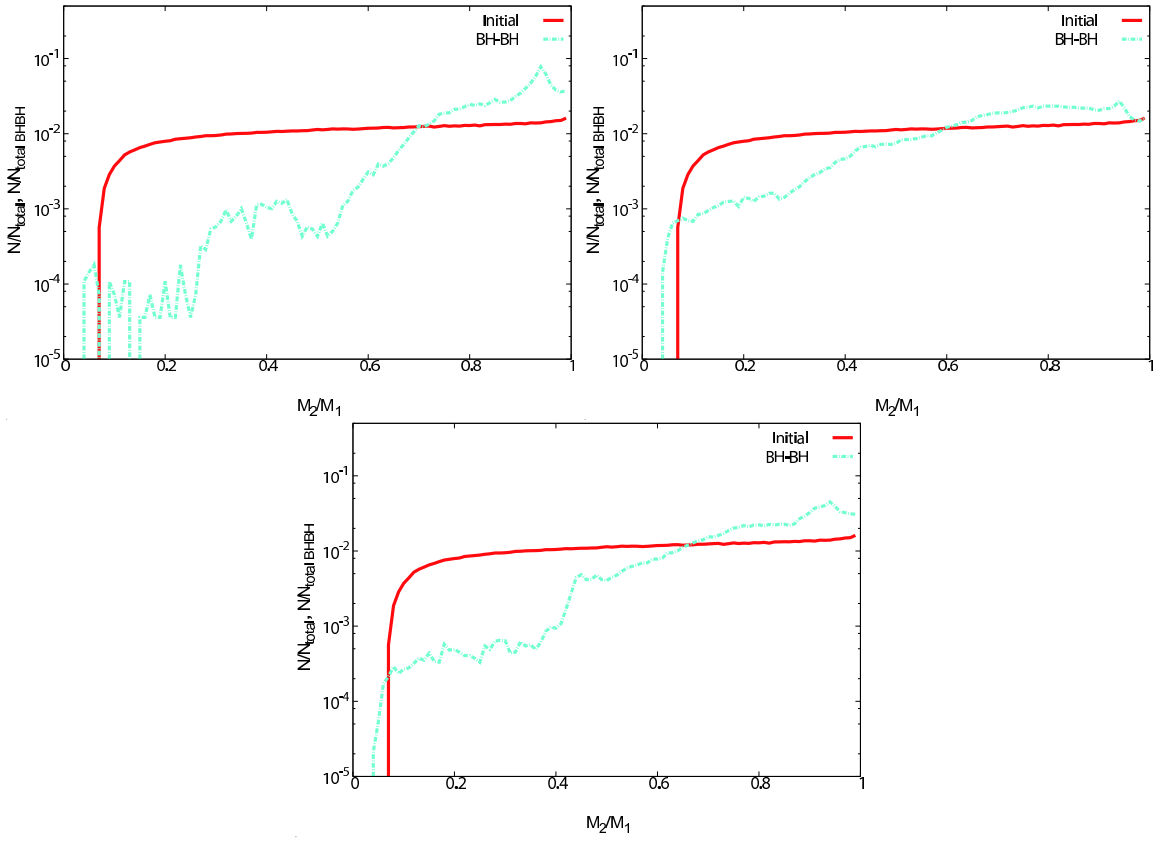

Fig. 4: The distributions of mass ratio $M_2/M_1 \leq 1$ for $\alpha\lambda = 0.01$ model (top-left), $\alpha\lambda = 0.1$ model (top-right) and $\alpha\lambda = 10$ model (bottom). The figures are same as Figure 1 but for $\alpha\lambda = 0.01$ model, $\alpha\lambda = 0.1$ model and $\alpha\lambda = 10$ model.

RLOF becomes not to be effective Third, a RLOF tends to finish early. The first effect make binaries evolve via a RLOF. However, the second and third effects have a negative impact

on the tendency to become equal mass. Thus, the mass ratio distributions of $\beta = 0.5$ and 1 models look like less change from that of our standard model.

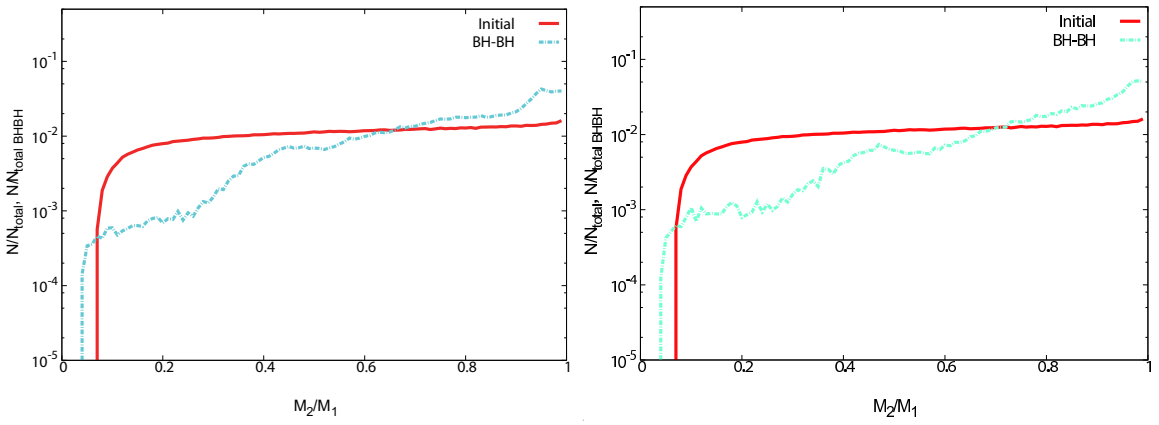

Fig. 5: The distributions of mass ratio $M_2/M_1 \leq 1$ for $\beta = 0.5$ model (left) and $\beta = 1$ model (right). The figures are same as Figure 1 but for $\beta = 0.5$ model and $\beta = 1$ model.

4. The spin distributions of binary black hole remnants

When the Pop III star becomes a BH, we calculate the BH's spin. If the estimated spin of the BH is more than the Thorne limit $q_{\rm Thorne} = 0.998$ [18], we assign the non-dimensional spin parameter $q = q_{\rm Thorne}$.

We ignore the spin up by the accretion during a mass transfer after the star became a BH. The reason is described as follows. The spin up by the accretion is calculated as

$$\begin{aligned} \delta q =& \frac{\delta J}{G M_{\rm BH}^2/c} \\ =& \sqrt{12}\frac{\delta M}{M_{\rm BH}}\,, \end{aligned} \tag{10}$$

where δJ, $M_{\rm BH}$, δM are the gain of angular momentum, the BH's mass, and the gain of BH's mass, respectively. Since the accretion rate of the BH during a RLOF is the Eddington rate, the gain of BH's mass is

$$\delta M \sim \dot{M}_{\rm Edd}\, t_{\rm life}\,, \tag{11}$$

where $t_{\rm life}$ is the lifetime of the Pop III star. The Eddington accretion rate is given by

$$\dot{M}_{\rm Edd} \sim 10^{-7} \left(\frac{M_{\rm BH}}{30\ M_\odot}\right)\ M_\odot\ {\rm yr}^{-1}\,, \tag{12}$$

and the lifetime of massive star is $t_{\rm life} \sim 1$ Myr. As the result, we have $\delta q \sim 0.01$, and the spin up by the accretion during a RLOF is negligible. On the other hand, in the case of a CE phase, the accretion rate during the CE phase is $\dot{M} \sim 10^{-3}\ M_\odot\ {\rm yr}^{-1}$ [19], and the timescale of the CE phase is about a thermal timescale of red giant $t_{\rm KH} \sim 10^2$ yr or less than the thermal timescale. As the result, we have $\delta q \leq 0.1$, and the spin up by the accretion during a CE phase is negligible, too.

Figures 6–15 show the spin distributions of merging BBHs and the cross section views of those spin distributions. The spins of merging Pop III BBH can be roughly classified into

three types: group 1 in which both BHs have high spins $q \sim 0.998$, group 2 in which both BHs have low spins, and group 3 in which the one of the pair has the high spin $q \sim 0.998$ and the other has low spin.

When the BH progenitor evolved via the CE phase, the Pop III BH has low spin, and vice versa. If the Pop III star which is a giant evolves via the CE phase, the Pop III star loses the envelope and almost all the angular momentum due to the envelope evaporation. On the other hand, if the Pop III star evolves without the CE phase, the Pop III star can have a high angular momentum. Therefore, in the group 1 progenitors evolve without the CE phase and the envelopes of the progenitors remain. In the group 2, both stars evolve via the CE phases and they lose their envelopes and almost all the angular momentum. In the group 3, the primary evolves via the CE phase, and the secondary evolves without the CE phase, or vice versa.

The IMF dependence of merging Pop III BBH spins is described as following (see Figs. 6, 7 and 8). The Pop III stars with masses $< 50 M_\odot$ evolve as a blue giant. Thus, in the case of the IMF that light stars are majority such as Salpeter IMF, the binaries tend to evolve only via the RLOF, not via the CE phase. Therefore, for the steeper IMF, we have larger numbers of merging Pop III BBHs which have high spins. Especially, in the case of Salpeter IMF the BBHs whose spins are $q_1 > 0.95$ and $q_2 > 0.95$, are about 40%.

As for the IEF dependence, there is no tendency like the mass ratio distribution (see Figs. 6, 9 and 10).

The dependence on the CE parameter can be considered as the following (see Figs. 6, 11, 12 and 13). In the $\alpha\lambda = 0.01$ model, almost all merging Pop III BBHs have high spins. About 60% of merging Pop III BBHs have $q_1 > 0.95$ and $q_2 > 0.95$ (i.e., group 1). This reason is that the progenitors which evolve via the CE phase always merge during the CE phase due to too small $\alpha\lambda$. Thus, the progenitors of merging Pop III BBHs in this model evolve only via the RLOF and they do not lose the angular momentum via the CE phase. In the case of $\alpha\lambda = 0.1$ model, the fraction of group 2 is lower than that of our standard model like the $\alpha\lambda = 0.01$ model. However, the fraction of group 1 is almost same as that of our standard model, and the fraction of group 3 is larger than that of our standard model not like a $\alpha\lambda = 0.01$ model. This reason is that although the progenitors which become CE phases more than one, merge during the CE phases due to small $\alpha\lambda$, the progenitors which become the CE phase at once, do not merge during the CE phase, and the Pop III BBHs which cannot merge within the Hubble time in our standard model, become to be able to merge within the Hubble time due to small $\alpha\lambda$. In the $\alpha\lambda = 10$ model, the shape of the spin distribution is almost same as that of our standard model. The difference of this model from our standard model is small increase of the fraction of group 2 because the progenitors which merge during the CE phase in our standard model, become to be able to survive due to large $\alpha\lambda$.

As for the β dependence (see Figs. 6, 14 and 15), Not only the stellar mass loss during the RLOF but also the criterion of the dynamically unstable mass transfer such as a CE phase are changed by β. In $\beta = 0.5$ model, the fraction of group 1 is larger than that of our standard model because in this model the progenitors more hardly become the CE phase than those of our standard model. In the $\beta = 1$ model, the fraction of group 1 is larger than that of our standard model like a $\beta = 0.5$ model. However, the fraction of group 1 is smaller than that of $\beta = 0.5$ model because in this model the progenitors lose a lot of angular

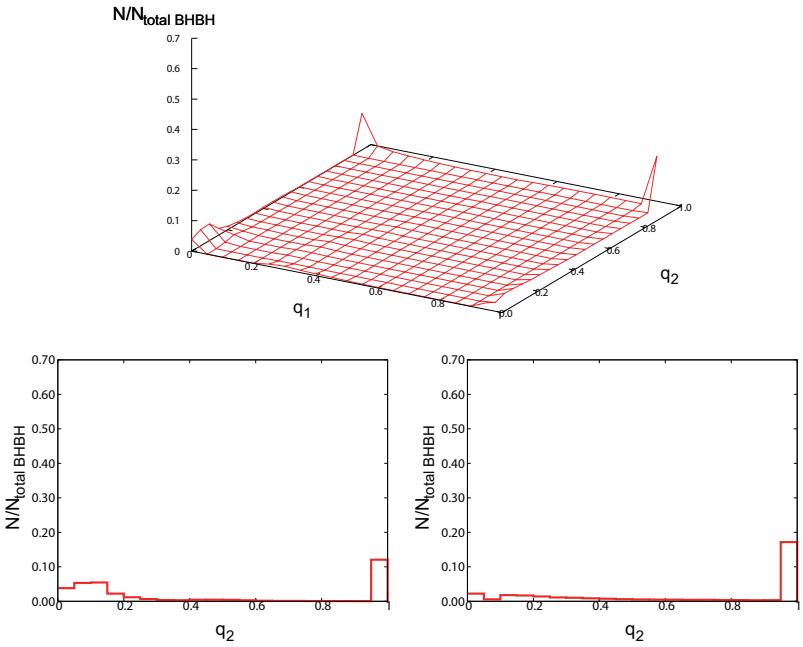

(a) $0 < q_1 < 0.05$ (b) $0.95 < q_1 < 0.998$

Fig. 6: (Top) The distribution of spin parameters for our standard model. This figure shows the distribution of spin parameters when each star becomes BH. q_1 and q_2 are the spin parameters of the primary and the secondary BHs, respectively. This distribution when the binaries become merging BBHs is normalized by the total merging BBH number $N_{\rm total\,BHBH} = 128897$ with the grid separation being $\Delta q_1 = \Delta q_2 = 0.05$. (Bottom) Cross section views of distribution of spin parameter for our standard model. (a) The distribution of q_2 for $0 < q_1 < 0.05$. We can see that q_2 distribution has bimodial peaks at $0 < q_2 < 0.15$ and $0.95 < q_2 < 0.998$. (b) The distribution of q_2 for $0.95 < q_1 < 0.998$. We see that the large value of q_2 is the majority so that there is a group in which both q_1 and q_2 are large.

momentum during the RLOF due to high β. In this model, since the mass transfer cannot become dynamically unstable, the progenitors of group 2 become the CE phase when the primary and secondary become a giant at the same time, and merge. On the other hand, the progenitors of group 3 become the CE phase when the secondary merges the primary giant due to initial eccentricity.

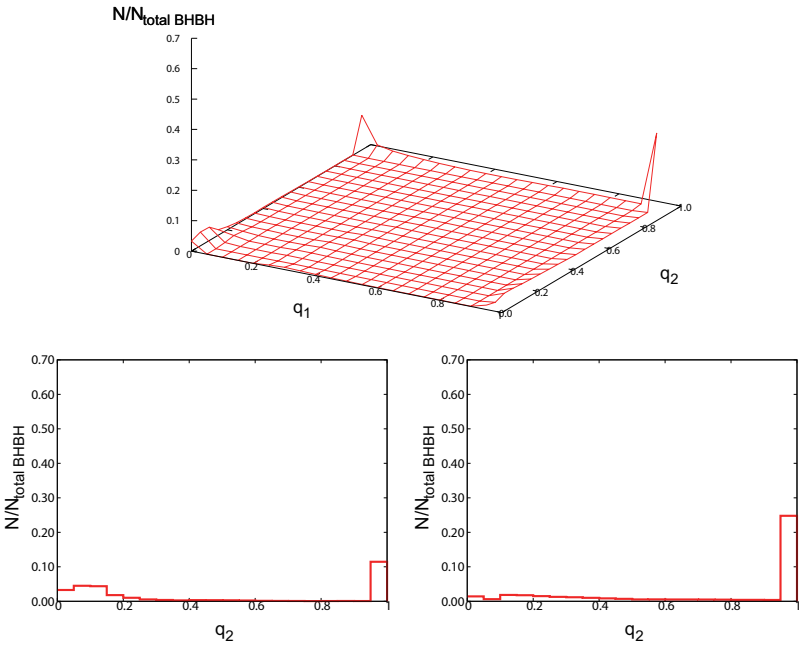

(a) $0 < q_1 < 0.05$ (b) $0.95 < q_1 < 0.998$

Fig. 7: (Top) The distribution of spin parameters for IMF: logflat model. $N_{\text{total BHBH}} = 87596$. (Bottom) Cross section views of distribution of spin parameter for IMF: logflat model. These figures are same as Figure 6 but for IMF: logflat model.

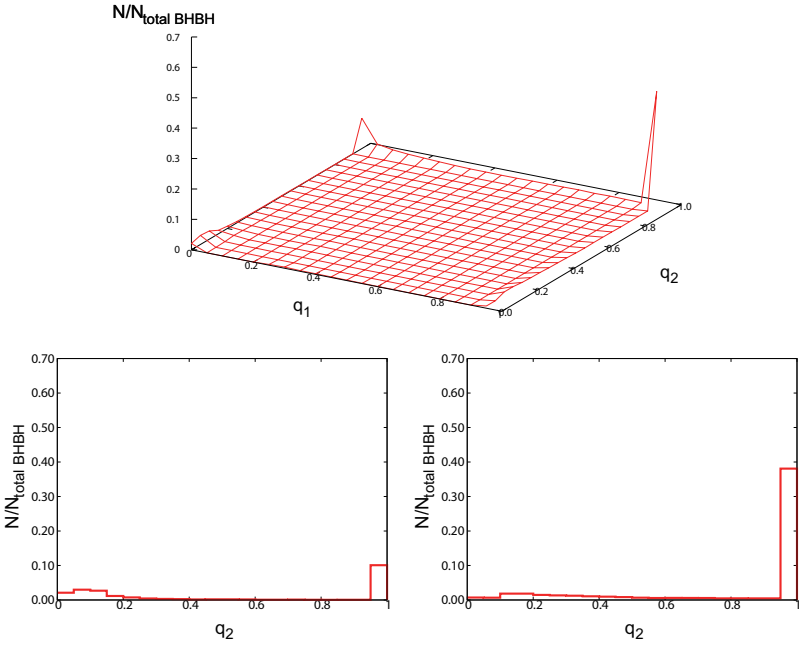

(a) $0 < q_1 < 0.05$ (b) $0.95 < q_1 < 0.998$

Fig. 8: (Top) The distribution of spin parameters for IMF: Salpeter model. $N_{\text{total BHBH}} = 28376$. (Bottom) Cross section views of distribution of spin parameter for IMF: Salpeter model. This figure is same as Figure 6 but for IMF: Salpeter model.

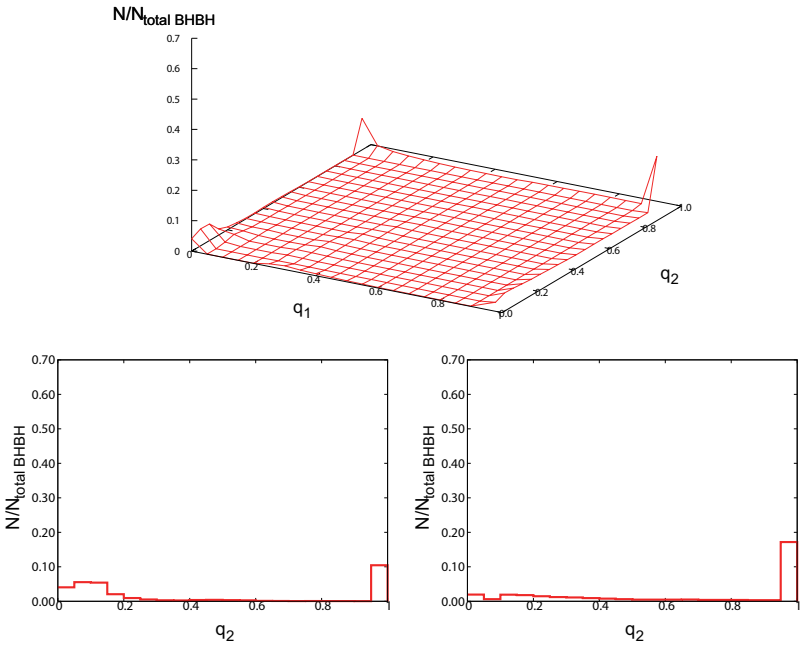

(a) $0 < q_1 < 0.05$ (b) $0.95 < q_1 < 0.998$

Fig. 9: (Top) The distribution of spin parameters for IEF: $e = $ const. model. $N_{\rm total\,BHBH} = 124711$. (Bottom) Cross section views of distribution of spin parameter for IEF: $e = $ const. model. This figure is same as Figure 6 but for IEF: $e = $ const. model.

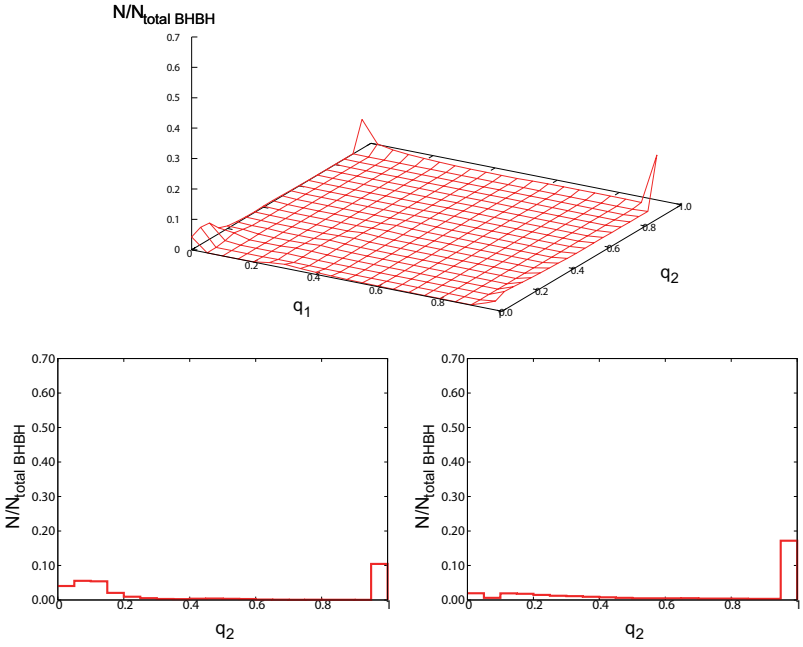

(a) $0 < q_1 < 0.05$ (b) $0.95 < q_1 < 0.998$

Fig. 10: (Top) The distribution of spin parameters for IEF: $e^{-0.5}$ model. $N_{\rm total\,BHBH} = 121495$. (Bottom) Cross section views of distribution of spin parameter for IEF: $e^{-0.5}$ model. This figure is same as Figure 6 but for IEF: $e^{-0.5}$ model.

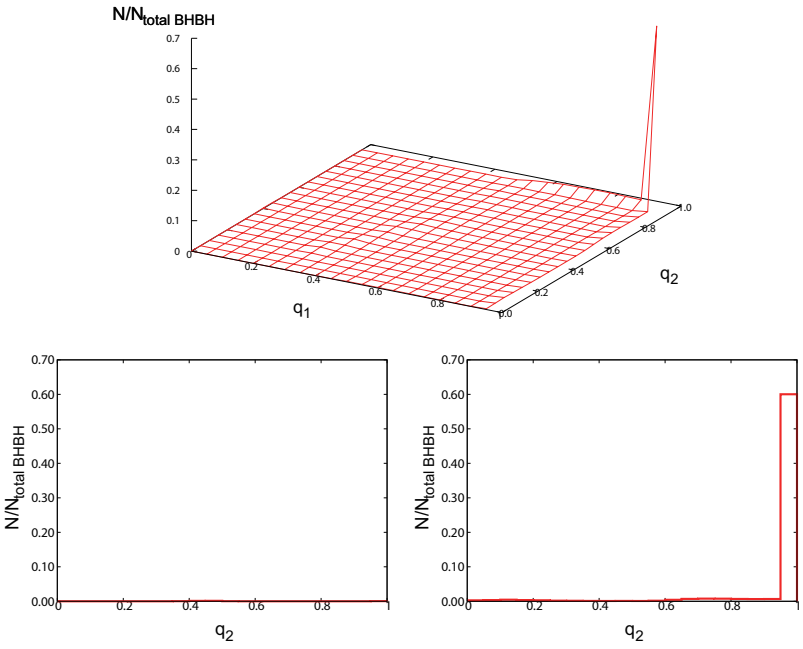

(a) $0 < q_1 < 0.05$ (b) $0.95 < q_1 < 0.998$

Fig. 11: (Top) The distribution of spin parameters for $\alpha\lambda = 0.01$ model. $N_{\rm total\,BHBH} = 27790$. (Bottom) Cross section views of distribution of spin parameter for $\alpha\lambda = 0.01$ model. This figure is same as Figure 6 but for $\alpha\lambda = 0.01$ model.

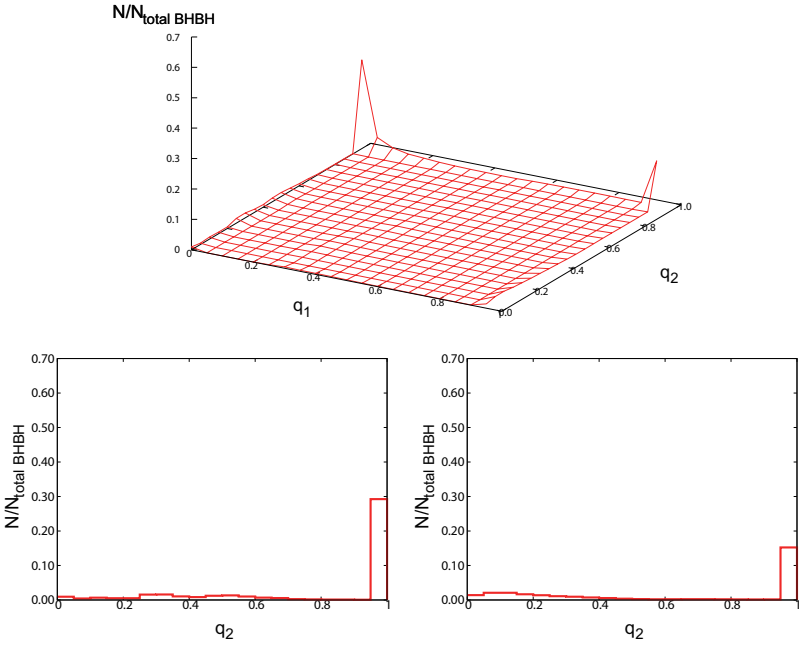

(a) $0 < q_1 < 0.05$ (b) $0.95 < q_1 < 0.998$

Fig. 12: (Top) The distribution of spin parameters for $\alpha\lambda = 0.1$ model. $N_{\rm total\,BHBH} = 124834$. (Bottom) Cross section views of distribution of spin parameter for $\alpha\lambda = 0.1$ model. This figure is same as Figure 6 but for $\alpha\lambda = 0.1$ model.

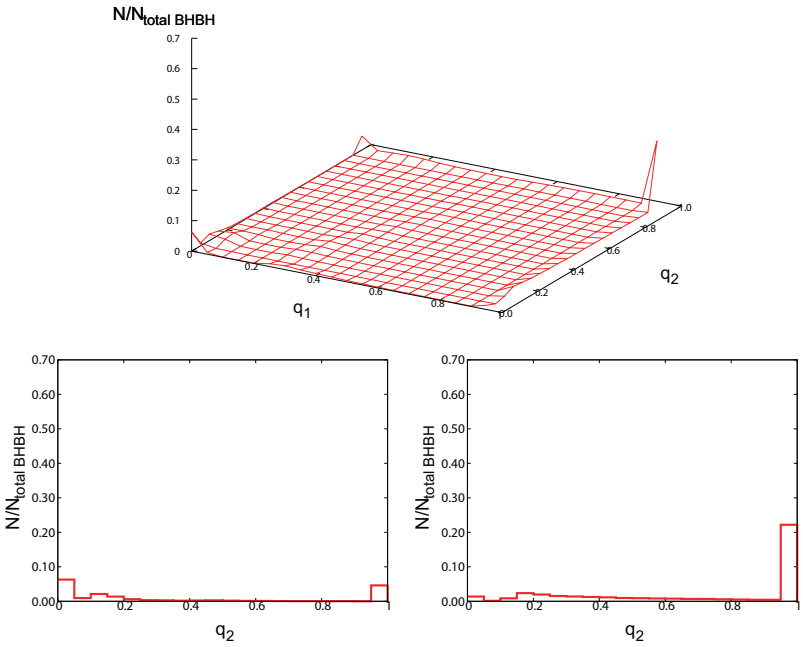

(a) $0 < q_1 < 0.05$ (b) $0.95 < q_1 < 0.998$

Fig. 13: (Top) The distribution of spin parameters for $\alpha\lambda = 10$ model. $N_{\rm total\,BHBH} = 93731$. (Bottom) Cross section views of distribution of spin parameter for $\alpha\lambda = 10$ model. This figure is same as Figure 6 but for $\alpha\lambda = 10$ model.

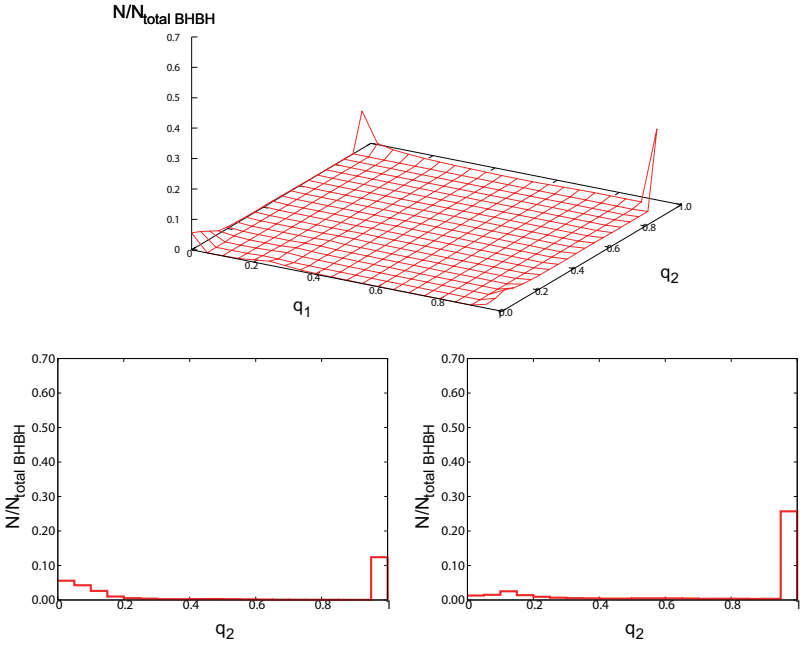

(a) $0 < q_1 < 0.05$ (b) $0.95 < q_1 < 0.998$

Fig. 14: (Top) The distribution of spin parameters for $\beta = 0.5$ model. $N_{\rm total\,BHBH} = 126093$. (Bottom) Cross section views of distribution of spin parameter for $\beta = 0.5$ model. This figure is same as Figure 6 but for $\beta = 0.5$ model.

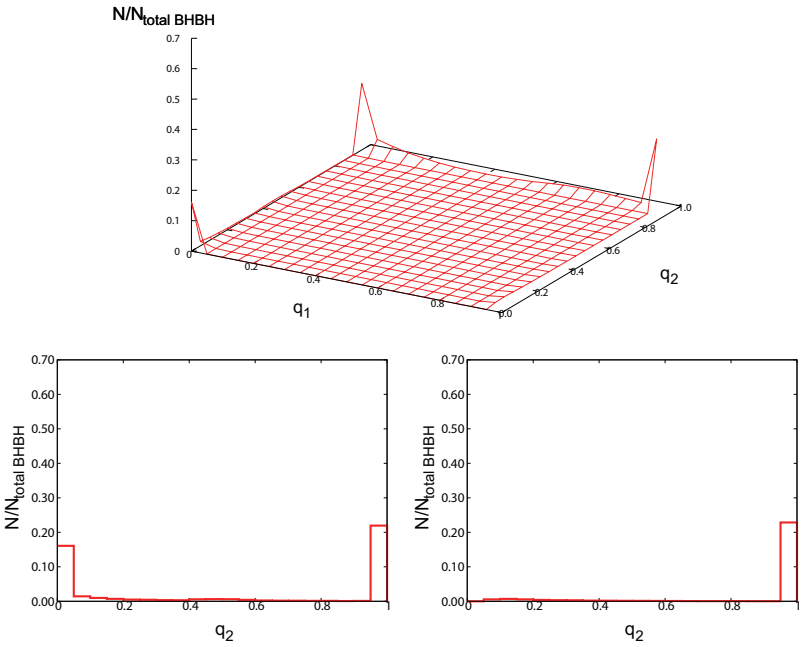

(a) $0 < q_1 < 0.05$ (b) $0.95 < q_1 < 0.998$

Fig. 15: (Top) The distribution of spin parameters for $\beta = 1$ model. $N_{\rm total\,BHBH} = 57028$. (Bottom) Cross section views of distribution of spin parameter for $\beta = 1$ model. This figure is same as Figure 6 but for $\beta = 1$ model.

5. Remnant and event rate for ringdown gravitational waves

5.1. Remnant mass and spin

Based on Ref. [11] (see also Refs. [20, 21]), we calculate the remnant mass M_f and spin q_f from given BH binary parameters, M_1, M_2, q_1 and q_2 (see Ref. [4] for the detailed discussion). The remnant mass and spin for each case is show in Figs. 16–25. Here, we have normalized the distribution, and used binning with $\Delta M_f = 10\,M_\odot$ for M_f and $\Delta q_f = 0.1$ (thick, red) and 0.02 (thin, blue) for q_f.

The IMF dependence shown in Figs. 16, 17 and 18 is described as following for the remnant mass and spin. When we treat the steeper IMF, we have a lower number of high mass remnants. On the other hand, the number of high spin remnants increase slightly in the steeper IMF cases. This is because in the steeper IMF models we have a large number of progenitors with mass smaller than 50 $M_\odot$.

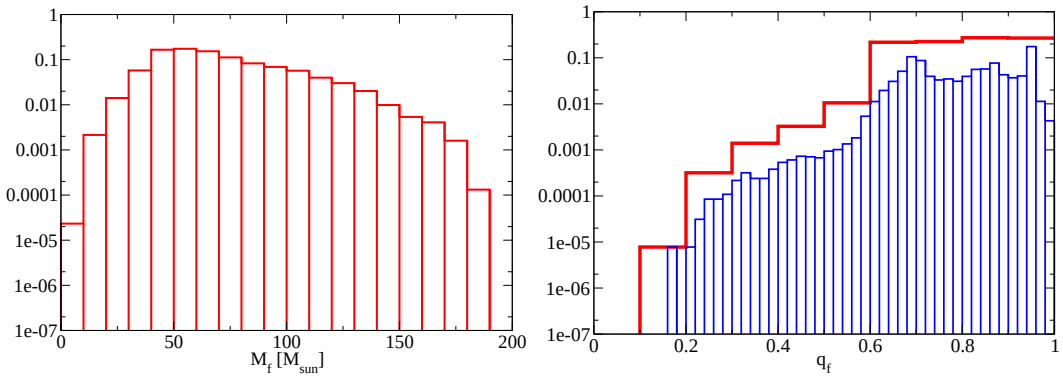

Fig. 16: The remnant mass M_f (left) and spin q_f (right) for our standard model.

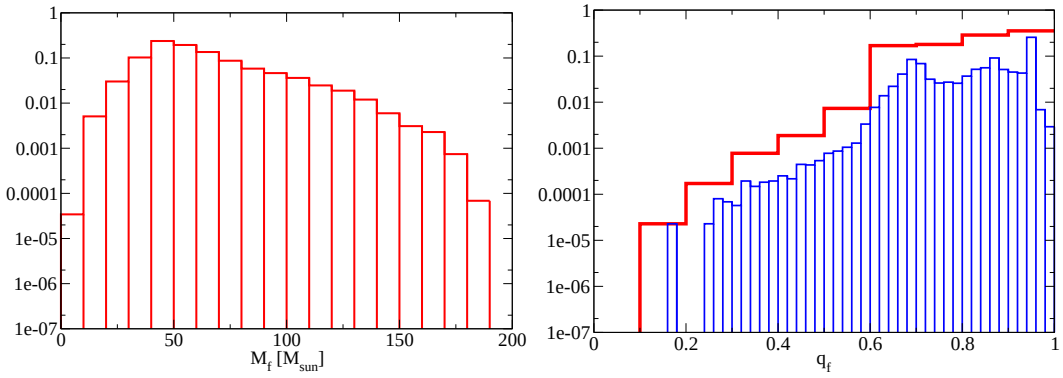

Fig. 17: The remnant mass M_f (left) and spin q_f (right) for IMF: logflat model.

As for the IEF dependence, we find that in Figs. 16, 19 and 20 there is no strong tendency.

Next, from Figs. 16, 21, 22 and 23 the CE parameter dependence is described as following. In the $\alpha\lambda = 0.01$ model, the maximum of the remnant mass becomes much smaller than that of our standard model. This is because the high mass progenitors merge during a CE phase due to too small $\alpha\lambda$, As for the remnant spin, we do not have remnant spins which

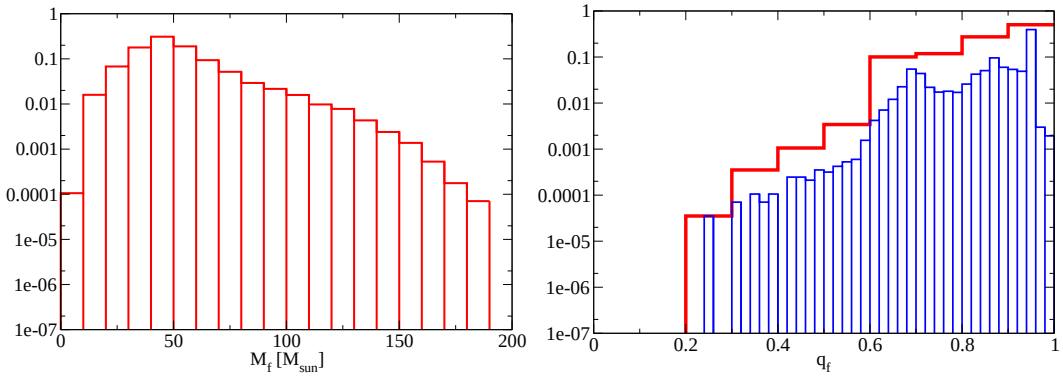

Fig. 18: The remnant mass M_f (left) and spin q_f (right) for IMF: Salpeter model.

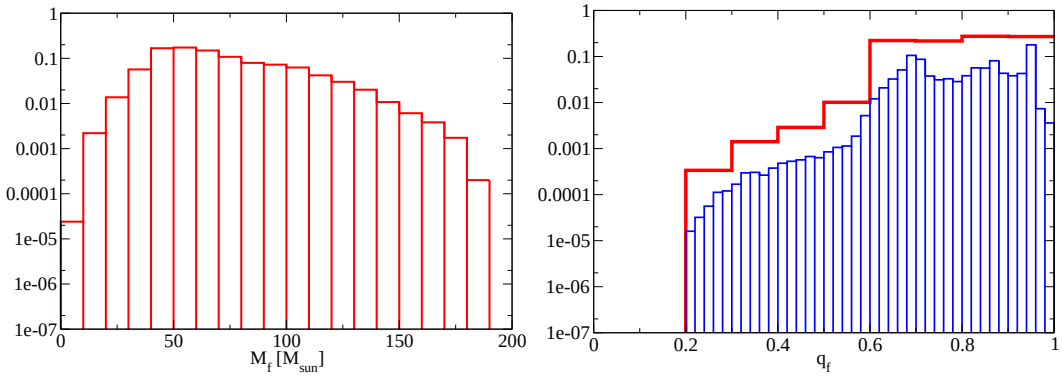

Fig. 19: The remnant mass M_f (left) and spin q_f (right) for IEF: e =const model.

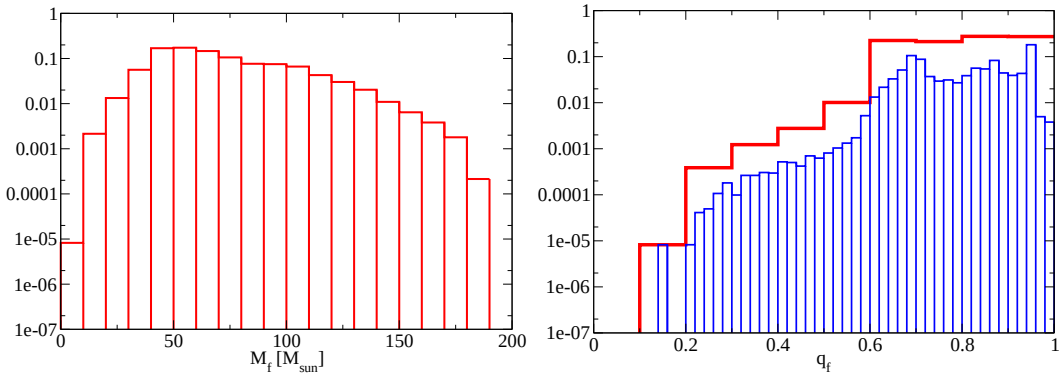

Fig. 20: The remnant mass M_f (left) and spin q_f (right) for IEF: $e^{-0.5}$ model.

are smaller than 0.55 since BBHs tend to be equal mass. If a light BH falls into a nonspining massive BH, the remnant BH can have a small spin ($q_f < 0.6$). However, in the above model many BBHs are equal mass. In the $\alpha\lambda = 0.1$ model, the maximum remnant mass is smaller than that of our standard model again. In this model, the fraction of the remnant spins with $0.7 < q_f < 0.8$ is larger than that for our standard model because the fraction of group 3 in this model is larger than that of our standard model. In the $\alpha\lambda = 10$ model, the maximum

remnant mass is larger than that of our standard model. This is because the high mass progenitors which tend to become a CE phase, can survive more easily during the CE phase than those of our standard model.

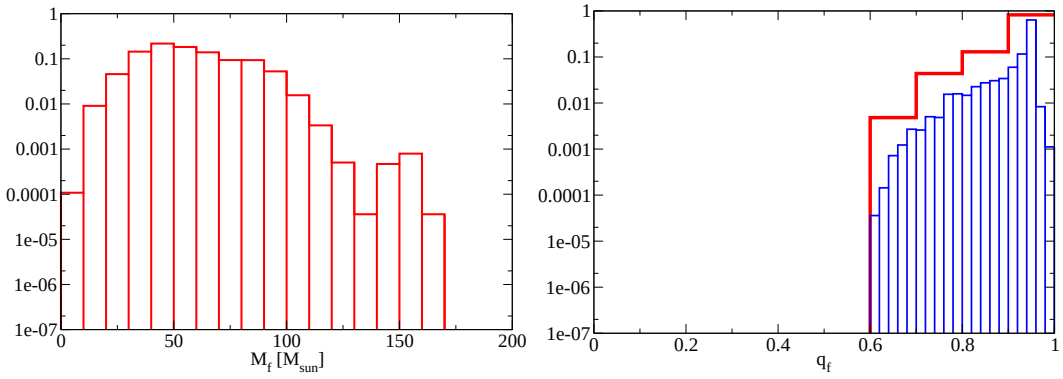

Fig. 21: The remnant mass M_f (left) and spin q_f (right) for $\alpha\lambda = 0.01$ model.

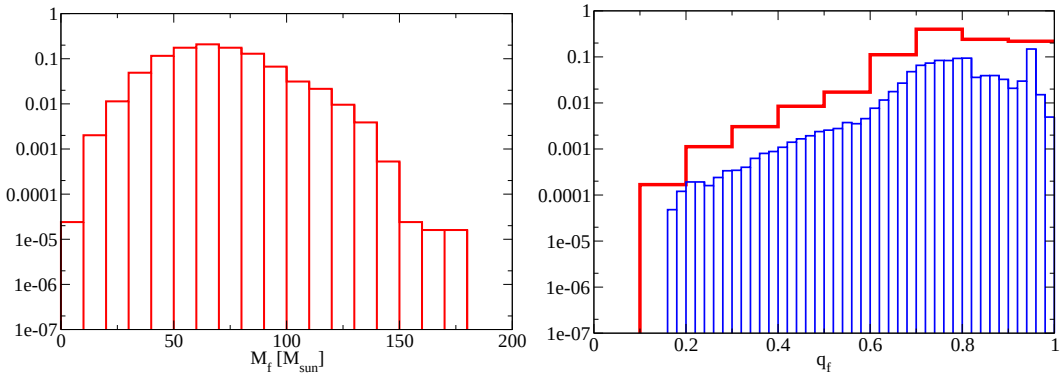

Fig. 22: The remnant mass M_f (left) and spin q_f (right) for $\alpha\lambda = 0.1$ model.

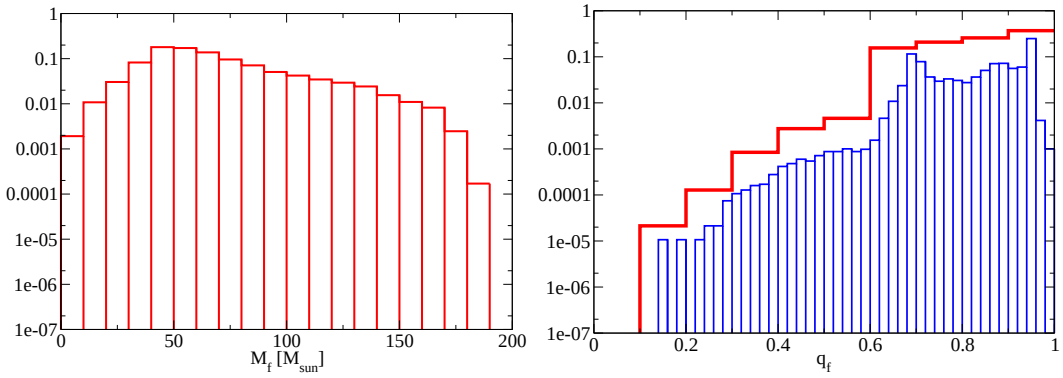

Fig. 23: The remnant mass M_f (left) and spin q_f (right) for $\alpha\lambda = 10$ model.

As for the β dependence we find that from Figs. 16, 24 and 25 the maximum of remnant mass becomes lower for the higher β, due to the mass loss during a RLOF.

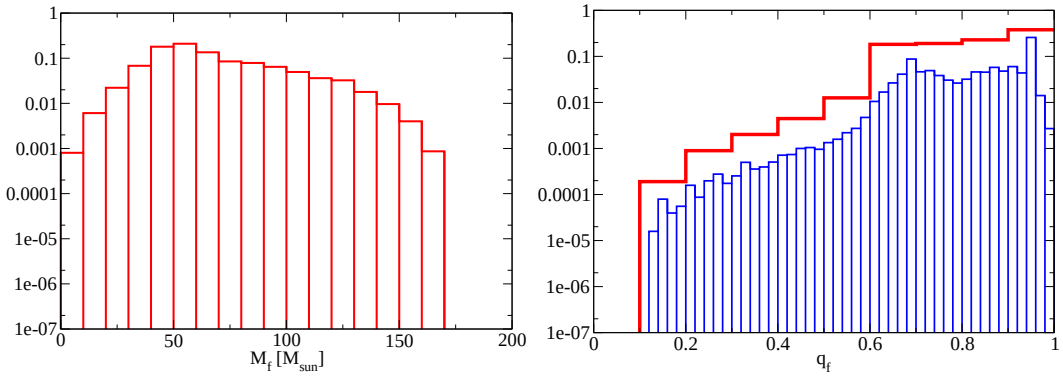

Fig. 24: The remnant mass M_f (left) and spin q_f (right) for $\beta = 0.5$ model.

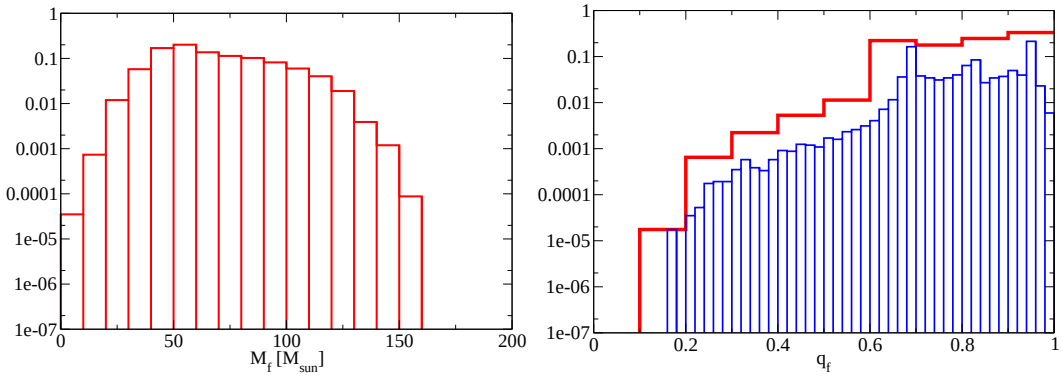

Fig. 25: The remnant mass M_f (left) and spin q_f (right) for $\beta = 1$ model.

5.2. Event rates for ringdown gravitational waves

To estimate the event rate for ringdown gravitational waves, it is necessary to have the merger rate density of Pop III BBHs. The merger rate density R_m [$\mathrm{Myr}^{-1}\mathrm{Mpc}^{-3}$] has been derived for various models in Ref. [6], and can be approximated by a fitting formula for low redshift. This is summarized in Table 2. In practice, we have considered the fitting for R_m in terms of the redshift z up to $z = 2$, but the above R_m is derived by using $z \propto D$ where D denotes the (luminosity) distance, because we use it only up to $z \sim 0.2$ in this paper.

Using Ref. [22], we calculate the angle averaged signal-to-noise ratio (SNR) as

$$\mathrm{SNR} = \sqrt{\frac{8}{5}}\frac{4\eta}{F(q_f)}\sqrt{\frac{\epsilon_r M_f}{S_n(f_c)}}\frac{M_f}{D}\,, \tag{13}$$

where we assume $\epsilon_r = 3\%$ of the total mass energy radiated in the ringdown phase. Note that for simplicity, any effect of the cosmological distance is ignored here. The symmetric

Table 2: Fitting formulas of the merger rate density R_m [$\mathrm{Myr}^{-1}\mathrm{Mpc}^{-3}$] for low redshift in the center column. Here, D denotes the (luminosity) distance. In the right column, the event rates [yr^{-1}] divided by dependence on the star formation rate $\mathrm{SFR_p}$ and the fraction of the binary $\mathrm{f_b}$ are shown for each model. We consider the events with SNR > 8 for the KAGRA detector here.

Model	R_m [$\mathrm{Myr}^{-1}\mathrm{Mpc}^{-3}$]	SNR > 8
Standard	$0.024 + 0.0080\ (D/1\,\mathrm{Gpc})$	446
IMF: logflat	$0.023 + 0.0064\ (D/1\,\mathrm{Gpc})$	255
IMF: Salpeter	$0.014 + 0.0034\ (D/1\,\mathrm{Gpc})$	61.5
IEF: e =const	$0.023 + 0.0075\ (D/1\,\mathrm{Gpc})$	452
IEF: $e^{-0.5}$	$0.022 + 0.0071\ (D/1\,\mathrm{Gpc})$	451
$\alpha\lambda = 0.01$	$0.0024 + 0.0018\ (D/1\,\mathrm{Gpc})$	5.87
$\alpha\lambda = 0.1$	$0.019 + 0.0089\ (D/1\,\mathrm{Gpc})$	146
$\alpha\lambda = 10$	$0.017 + 0.0066\ (D/1\,\mathrm{Gpc})$	372
$\beta = 0.5$	$0.030 + 0.0099\ (D/1\,\mathrm{Gpc})$	499
$\beta = 1$	$0.017 + 0.0029\ (D/1\,\mathrm{Gpc})$	158

mass ratio $\eta = M_1M_2/(M_1+M_2)^2$ is evaluated from the inspiral phase, and

$$F(q_f) = 1.5251 - 1.1568(1-q_f)^{0.1292}\,, \quad f_c = \frac{1}{2\pi M_f}F(q_f)\,, \tag{14}$$

are obtained from the remnant BH's mass and spin (see Ref. [23]). We evaluate the above SNR of the QNM GWs in the expected KAGRA noise curve $S_n(f)$ [9, 10] [bKAGRA, VRSE(D) configuration] (see Ref. [4] for the detailed calculation). This noise curve is presented in Ref. [26], and we use the fitting noise curve obtained in Ref. [24], based on Ref. [26]. Then, the event rate for a given SNR is derived by using the merger rate density in Table 2. In the right column of Table 2, we present the event rate with SNR>8. Here, the event rates [yr^{-1}] have been divided by dependence on the star formation rate $\mathrm{SFR_p}$ and the fraction of the binary $\mathrm{f_b}$

Next, using the event with SNR>35, we summarize various event rates in Tables 3 and 4. Table 3 shows the total event rates [yr^{-1}] divided by dependence on the star formation rate $\mathrm{SFR_p}$ and the fraction of the binary $\mathrm{f_b}$ for 10 models, and those for the remnant BH with $q_f > 0.7$ and 0.95.

In Table 4, we present the detection rate [yr^{-1}] divided by dependence on the star formation rate $\mathrm{SFR_p}$ and the fraction of the binary $\mathrm{f_b}$ as a function of the lower limit of the solid angle of a sphere $4\pi C$ by which we can estimate the contribution of the ergoregion. The relation between this C and the spin parameter q was obtained in Ref. [27] (see also resent studies [25, 27–29]).

6. Discussions

In this paper, we extended our previous work [4] (standar model in this paper) with various parameter dependence of the Pop III binary population synthesis calculation. As shown in the right column of Table 2, the detection rate with SNR$>$

Table 3: The total event rate [yr^{-1}] divided by dependence on the star formation rate $\mathrm{SFR_p}$ and the fraction of the binary $\mathrm{f_b}$ for each model and those for the final $q_f > 0.7$ and 0.95 BHs in the case of SNR > 35 for the KAGRA detector.

Model	all	$0.7 < q_f$	$0.95 < q_f$
Standard	3.73	2.45	0.0260
IMF: logflat	2.17	1.41	0.0152
IMF: Salpeter	0.530	0.337	0.00300
IEF: e =const	3.80	2.38	0.0248
IEF: $e^{-0.5}$	3.82	2.38	0.0228
$\alpha\lambda = 0.01$	0.0463	0.0411	0.00268
$\alpha\lambda = 0.1$	1.23	0.864	0.0114
$\alpha\lambda = 10$	2.96	2.16	0.0372
$\beta = 0.5$	4.21	3.29	0.0157
$\beta = 1$	1.58	0.705	0.0128

Table 4: The event rates [yr^{-1}] divided by dependence on the star formation rate $\mathrm{SFR_p}$ and the fraction of the binary $\mathrm{f_b}$ as a function of the lower limit of the solid angle of a sphere $4\pi C$ where the QNM is mainly emitted from the ergoregion, in the case of SNR> 35 for the KAGRA detector.

Model	$0.5 < C$	$0.7 < C$	$0.9 < C$	$0.95 < C$	$0.97 < C$	$0.99 < C$
Standard	2.23	1.10	0.356	0.162	0.117	0.0780
IMF: logflat	1.29	0.621	0.207	0.102	0.0683	0.0454
IMF: Salpeter	0.309	0.145	0.0489	0.0234	0.0156	0.00960
IEF: e =const	2.18	0.998	0.288	0.132	0.0955	0.0621
IEF: $e^{-0.5}$	2.15	0.936	0.237	0.115	0.0825	0.0518
$\alpha\lambda = 0.01$	0.0399	0.0318	0.0131	0.00966	0.00839	0.00503
$\alpha\lambda = 0.1$	0.820	0.391	0.135	0.0609	0.0390	0.0222
$\alpha\lambda = 10$	2.01	1.09	0.470	0.307	0.246	0.187
$\beta = 0.5$	3.09	0.979	0.294	0.127	0.0990	0.0292
$\beta = 1$	0.666	0.405	0.0278	0.0218	0.0187	0.0141

8 for the second generation GW detectors such as KAGRA was obtained as $5.9 - 500$ events yr^{-1} $(\mathrm{SFR_p}/(10^{-2.5}\ M_\odot\ \mathrm{yr}^{-1}\ \mathrm{Mpc}^{-3})) \cdot ([\mathrm{f_b}/(1+\mathrm{f_b})]/0.33)$ between 10 models. Recently, Kushnir et al. [30] have discussed whether the BH's spin constrains the binary evolution path in the case of Pop I and Pop II binaries. If we detect a lot of Pop III BBH mergers, we might be able to constrain the Pop III binary evolution paths not only by the mass distribution but also by the spin distribution, too.

One of the interesting output from the QNM GWs is whether we can confirm the ergoregion of the Kerr BH. From Table 4, the event rate for the confirmation of $> 50\%$ of the ergoregion

is $0.040 - 3.1$ events yr^{-1} (SFR$_{\rm p}$/($10^{-2.5}$ $M_\odot$ yr^{-1} Mpc^{-3})) $\cdot$ ([f$_{\rm b}$/(1 + f$_{\rm b}$)]/0.33) with SNR$>$ 35.

When we consider to extract the rotational energy of BHs such as Penrose process [31] and the Blanford-Znajek process [32], we want to observe highly spinning remnant BHs. For remnant BH's spins $q_f > 0.95$, the event rate with SNR$>$ 35 is $0.0027 - 0.037$ events yr^{-1} (SFR$_{\rm p}$/($10^{-2.5}$ $M_\odot$ yr^{-1} Mpc^{-3})) $\cdot$ ([f$_{\rm b}$/(1 + f$_{\rm b}$)]/0.33) in the KAGRA detector from Table 3. A third-generation GW observatory, the Einstein Telescope (ET) [33] will have an improvement of the sensitivity by about a factor 10 from the second generations detectors. This means that we have roughly 1000 times higher than the current expected event rates, and for example, the ringdown event rate with $q_f > 0.95$ will become

$$3 - 30 \text{ events yr}^{-1} \left(\frac{\text{SFR}_{\rm p}}{10^{-2.5}\ \text{M}_\odot\ \text{yr}^{-1}\ \text{Mpc}^{-3}}\right) \cdot \left(\frac{\text{f}_{\rm b}/(1+\text{f}_{\rm b})}{0.33}\right) \left(\frac{\epsilon_r}{0.03}\right)^{1/2} . \qquad (15)$$

Here, we have introduced ϵ_r as the fraction of the BH mass radiated in the ringdown phase, and assumed $\epsilon_r = 3\%$ to calculate the SNR and the event rates in this paper. If $\epsilon_r = 0.3\%$, we will still have a possibility to detect the QNM GWs from highly spinning remnant BHs.

Finally, Pop III BBH mergers is possible to be a target for space-based GW detectors such as eLISA [34] and DECIGO [35]. The study in this direction is one of our future works.

Acknowledgment

This work was supported by MEXT Grant-in-Aid for Scientific Research on Innovative Areas, "New Developments in Astrophysics Through Multi-Messenger Observations of Gravitational Wave Sources", Nos. 24103001 and 24103006 (HN, TN, TT), JSPS Grant-in-Aid for Scientific Research (C), No. 16K05347 (HN), and the Grant-in-Aid from the Ministry of Education, Culture, Sports, Science and Technology (MEXT) of Japan, No. 15H02087 (TN, TT).

References

[1] V. Cardoso, E. Franzin and P. Pani, Phys. Rev. Lett. **116**, 171101 (2016) [arXiv:1602.07309 [gr-qc]].
[2] R. P. Kerr, Phys. Rev. Lett. **11**, 237 (1963).
[3] E. Berti *et al.*, Class. Quant. Grav. **32**, 243001 (2015) [arXiv:1501.07274 [gr-qc]].
[4] T. Kinugawa, H. Nakano and T. Nakamura, Prog. Theor. Exp. Phys. (2016), 031E01 [arXiv:1601.07217 [astro-ph.HE]].
[5] T. Kinugawa, K. Inayoshi, K. Hotokezaka, D. Nakauchi and T. Nakamura, Mon. Not. Roy. Astron. Soc. **442**, 2963 (2014) [arXiv:1402.6672 [astro-ph.HE]].
[6] T. Kinugawa, A. Miyamoto, N. Kanda and T. Nakamura, Mon. Not. Roy. Astron. Soc. **456**, no. 1, 1093 (2016) [arXiv:1505.06962 [astro-ph.SR]].
[7] J. Aasi *et al.* [LIGO Scientific Collaboration], Class. Quant. Grav. **32**, 074001 (2015) [arXiv:1411.4547 [gr-qc]].
[8] F. Acernese *et al.* [VIRGO Collaboration], Class. Quant. Grav. **32**, 024001 (2015) [arXiv:1408.3978 [gr-qc]].
[9] K. Somiya [KAGRA Collaboration], Class. Quant. Grav. **29**, 124007 (2012) [arXiv:1111.7185 [gr-qc]].
[10] Y. Aso *et al.* [KAGRA Collaboration], Phys. Rev. D **88**, 043007 (2013) [arXiv:1306.6747 [gr-qc]].
[11] J. Healy, C. O. Lousto and Y. Zlochower, Phys. Rev. D **90**, 104004 (2014) [arXiv:1406.7295 [gr-qc]].
[12] J. R. Hurley, C. A. Tout and O. R. Pols, Mon. Not. Roy. Astron. Soc. **329**, 897 (2002) [astro-ph/0201220].
[13] `http://astronomy.swin.edu.au/~jhurley/`
[14] S. Hirano, T. Hosokawa, N. Yoshida, H. Umeda, K. Omukai, G. Chiaki and H. W. Yorke, Astrophys. J. **781**, 60 (2014) [arXiv:1308.4456 [astro-ph.CO]].
[15] H. Susa, K. Hasegawa and N. Tominaga, Astrophys. J. **792**, 32 (2014) [arXiv:1407.1374 [astro-ph.GA]].
[16] P. Eggleton, *Evolutionary Processes in Binary and Multiple Stars* (Cambridge University Press, Cambridge, UK, 2011)

[17] R. F. Webbink, Astrophys. J. **277**, 355 (1984).
[18] K. S. Thorne, Astrophys. J. **191**, 507 (1974).
[19] N. Ivanova *et al.*, Astron. Astrophys. Rev. **21**, 59 (2013) [arXiv:1209.4302 [astro-ph.HE]].
[20] E. Barausse, V. Morozova and L. Rezzolla, Astrophys. J. **758**, 63 (2012) [Astrophys. J. **786**, 76 (2014)] [arXiv:1206.3803 [gr-qc]].
[21] F. Hofmann, E. Barausse and L. Rezzolla, arXiv:1605.01938 [gr-qc].
[22] E. E. Flanagan and S. A. Hughes, Phys. Rev. D **57**, 4535 (1998) [gr-qc/9701039].
[23] E. Berti, V. Cardoso and C. M. Will, Phys. Rev. D **73**, 064030 (2006) [gr-qc/0512160].
[24] H. Nakano, T. Tanaka and T. Nakamura, Phys. Rev. D **92**, 064003 (2015) [arXiv:1506.00560 [astro-ph.HE]].
[25] T. Nakamura, H. Nakano and T. Tanaka, Phys. Rev. D **93**, 044048 (2016) [arXiv:1601.00356 [astro-ph.HE]].
[26] `http://gwcenter.icrr.u-tokyo.ac.jp/researcher/parameters`
[27] H. Nakano, T. Nakamura and T. Tanaka, Prog. Theor. Exp. Phys. (2016) 031E02 [arXiv:1602.02875 [gr-qc]].
[28] T. Nakamura and H. Nakano, Prog. Theor. Exp. Phys. (2016) 041E01 [arXiv:1602.02385 [gr-qc]].
[29] H. Nakano, N. Sago, T. Tanaka and T. Nakamura, arXiv:1604.08285 [gr-qc].
[30] D. Kushnir, M. Zaldarriaga, J. A. Kollmeier and R. Waldman, arXiv:1605.03839 [astro-ph.HE].
[31] R. Penrose, Riv. Nuovo Cim. **1**, 252 (1969) [Gen. Rel. Grav. **34**, 1141 (2002)].
[32] R. D. Blandford and R. L. Znajek, Mon. Not. Roy. Astron. Soc. **179**, 433 (1977).
[33] M. Punturo *et al.*, Class. Quant. Grav. **27**, 194002 (2010).
[34] P. A. Seoane *et al.* [eLISA Collaboration], arXiv:1305.5720 [astro-ph.CO].
[35] N. Seto, S. Kawamura and T. Nakamura, Phys. Rev. Lett. **87**, 221103 (2001) [astro-ph/0108011].

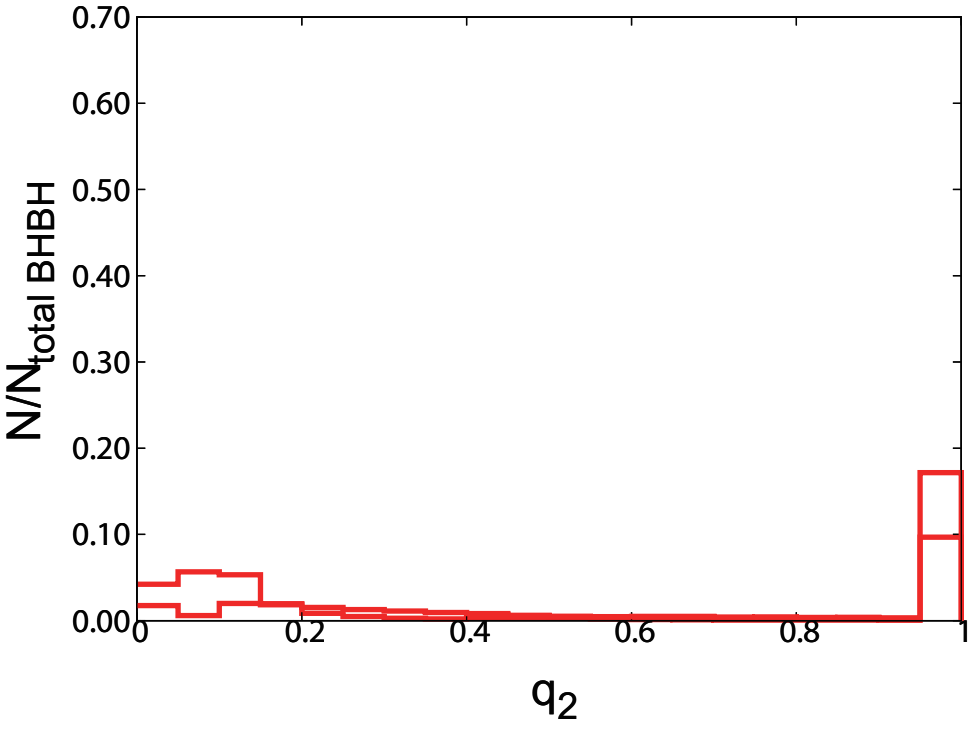
0.70
0.60
0.50
0.40
0.30
0.20
0.10
0.00
N/N_total BHBH
0
0.2
0.4
0.6
0.8
1
q_2